

A scheme for the detection of mixing processes in vacuum

François Fillion-Gourdeau,^{1,*} Catherine Lefebvre,^{1,†} and Steve MacLean^{1,2,‡}

¹*Université du Québec, INRS-Énergie, Matériaux et Télécommunications, Varennes, Québec, Canada J3X 1S2*

²*Institute for Quantum Computing, University of Waterloo, Waterloo, Ontario, Canada, N2L 3G1*

(Dated: December 6, 2024)

A scheme for the detection of photons generated by vacuum mixing processes is proposed. The strategy consists in the utilization of a high numerical aperture parabolic mirror which tightly focuses two co-propagating laser beams with different frequencies. This produces a very high intensity region in the vicinity of the focus, where the photon-photon nonlinear interaction can then induce new electromagnetic radiation by wave mixing processes. These processes are investigated theoretically. The field at the focus is obtained from the Stratton-Chu vector diffraction theory, which can accommodate any configuration of an incoming laser beam. The number of photons generated is evaluated for an incident radially polarized beam. It is demonstrated that using this field configuration, vacuum mixing processes could be detected with envisaged laser technologies.

With recent advances in laser technology, that enable unprecedented intensity levels (above 10^{20} W/cm² [1]), there has been a surge of interest in the study and discovery of Quantum Electrodynamics (QED) processes in laser physics [2]. One of the most important and surprising signatures of QED is the possibility of inducing wave mixing in the “vacuum”, whereby electromagnetic radiation of novel frequencies are generated from the interaction between photons. This phenomenon is very similar to processes occurring in nonlinear media, such as four-wave mixing, harmonic generation and the propagation in birefringent material. These are the result of the nonlinear polarization and magnetization characterizing the medium response to an external electromagnetic field. According to the QED effective action [3], an analogous feature also exists in vacuum owing to photon-photon interaction because these interactions also generate nonlinear polarization and magnetization [4, 5]. For relatively small field strengths obeying $|\mathbf{E}|, |\mathbf{B}| \ll E_S$ (where the Schwinger field is $E_S = 1.3 \times 10^{18}$ V/m), the leading order expression in the fine coupling constant $\alpha \approx 1/137$ of the vacuum response scales like $\sim \alpha^2$ and is cubic in the electromagnetic field. As a consequence, the effect is very weak for field strengths reached by current lasers and thus, it has eluded experimental verification so far [6]. Nevertheless, many observables have been studied and proposed theoretically to investigate the QED nonlinearity, taking advantage of the formal analogy with optics. These include four-wave mixing [4, 5], vacuum birefringence [7–10] and second harmonic generation [11]. All of these processes occur due to the fact that QED induces a cubic nonlinearity.

This work revisits one of the well-known mixing processes where two incident fields with different frequencies ω_1 and ω_2 interact with each other to generate harmonics (this study focuses on the generation of $\omega_a = 2\omega_1 - \omega_2$ and $\omega_b = 2\omega_2 - \omega_1$). The originality of this article resides in the field configuration considered, depicted in Fig. 1: the two laser beams are initially co-propagating and tightly focused by a parabolic mirror with a High Nu-

merical Aperture (HNA). A similar setup has been used in [12] to accelerate electrons. Mixing processes then occur close to the focal point where the electromagnetic radiation reaches its highest intensity. It will be shown that this geometry can increase the number of emitted photons significantly while circumventing some technical and experimental limitations.

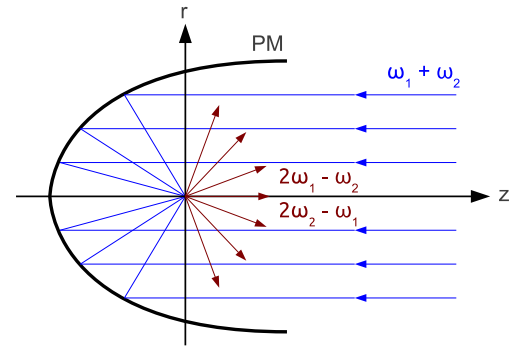


FIG. 1: Field configuration: an incident laser beam (blue) with co-propagating frequencies ω_1 and ω_2 is focused by a parabolic mirror (PM). At the focal point, the intensity of the electromagnetic radiation is the highest and photons of frequencies $\omega_a = 2\omega_1 - \omega_2$ and $\omega_b = 2\omega_2 - \omega_1$ (red) can be generated.

There have been many proposals to detect these mixing effects using other field configurations. One of the earlier works on this topic considered the four wave mixing process of three linearly polarized plane and Gaussian waves [4–6]. This was tested experimentally using two strong counterpropagating beams and one weaker beam, interacting at an angle [6]. It was concluded that the intensity level used in the experiment was not high enough to detect the QED effect, although it was possible to put an experimental upper limit on the photon-photon cross-section of $\sigma_{\text{QED}} < 1.5 \times 10^{-48}$ cm² [6]. Similar theoretical investigations have been performed, for other promising

field configurations, using the crossing of three Gaussian beams with optimized polarizations [13] and by considering the collision of two short pulses [14]. Recently, the generation of radiation from a single strongly focused beam was considered [15]. In this particular case, the nonlinearly induced field has the same frequency as the incident laser field. The two signals can be discriminated because the generated radiation has a field component orthogonal to the incident linearly polarized field.

In this article, the photon number and space distribution are evaluated for mixing processes occurring at the focus of the HNA parabola. The strategy to evaluate the photon distribution is divided in three main steps: 1. Fixing the incident field. 2. Calculation of the field close to the focal point. 3. Determination of the generated radiation. Each step will be detailed in the following. QED units in which $\hbar = c = m = \epsilon_0 = \mu_0 = 1$ (where m is the electron mass) and $e = \sqrt{4\pi\alpha}$ are used throughout the calculations.

The starting point of this work is the set of time-dependent Maxwell's equations given by

$$\frac{\partial \mathbf{B}(\mathbf{r}, t)}{\partial t} = -\nabla \times \mathbf{E}(\mathbf{r}, t), \quad \nabla \cdot \mathbf{B}(\mathbf{r}, t) = 0, \quad (1)$$

$$\frac{\partial \mathbf{D}(\mathbf{r}, t)}{\partial t} = \nabla \times \mathbf{H}(\mathbf{r}, t), \quad \nabla \cdot \mathbf{D}(\mathbf{r}, t) = 0, \quad (2)$$

where \mathbf{r} is the space coordinate, t is the time and \mathbf{E} and \mathbf{B} are the electric and magnetic fields, respectively. The displacement field \mathbf{D} and magnetizing field \mathbf{H} are given in terms of the polarization \mathbf{P} and magnetization \mathbf{M} as

$$\mathbf{D}(\mathbf{r}, t) = \mathbf{E}(\mathbf{r}, t) + \mathbf{P}(\mathbf{r}, t), \quad (3)$$

$$\mathbf{H}(\mathbf{r}, t) = \mathbf{B}(\mathbf{r}, t) - \mathbf{M}(\mathbf{r}, t). \quad (4)$$

So far, this corresponds exactly to classical electromagnetic theory in matter where the polarization and magnetization characterize the response of materials to the electromagnetic field. According to the QED effective action (Heisenberg-Euler action [3]), the “vacuum” also behaves in a similar way due to photon-photon interaction. In the weak field limit, when $|\mathbf{E}|, |\mathbf{B}| \ll E_S$, in the low photon energy limit, when $\hbar\omega \ll mc^2$, and for wavelengths smaller than the Compton wavelength [16], this action yields the Maxwell's equations described previously, with polarization and magnetization vector fields given by [3]

$$\mathbf{P}(\mathbf{r}, t) = a \left\{ 2 [\mathbf{E}^2(\mathbf{r}, t) - \mathbf{B}^2(\mathbf{r}, t)] \mathbf{E}(\mathbf{r}, t) + 7 [\mathbf{E}(\mathbf{r}, t) \cdot \mathbf{B}(\mathbf{r}, t)] \mathbf{B}(\mathbf{r}, t) \right\}, \quad (5)$$

$$\mathbf{M}(\mathbf{r}, t) = a \left\{ 2 [\mathbf{B}^2(\mathbf{r}, t) - \mathbf{E}^2(\mathbf{r}, t)] \mathbf{B}(\mathbf{r}, t) + 7 [\mathbf{E}(\mathbf{r}, t) \cdot \mathbf{B}(\mathbf{r}, t)] \mathbf{E}(\mathbf{r}, t) \right\}, \quad (6)$$

where the constant $a := \frac{4\alpha^2}{45}$. Maxwell's equations, along with the expression of the polarization and magnetization obtained from the QED effective action, govern the time evolution of the electric and magnetic fields with photon self-interaction. These equations (3)-(6) can be turned into wave equations for the electric and magnetic fields:

$$[\partial_t^2 - \nabla^2] \mathbf{E}(\mathbf{r}, t) = -\partial_t [\nabla \times \mathbf{M}(\mathbf{r}, t)] - \partial_t^2 \mathbf{P}(\mathbf{r}, t) + \nabla [\nabla \cdot \mathbf{P}(\mathbf{r}, t)], \quad (7)$$

$$[\partial_t^2 - \nabla^2] \mathbf{B}(\mathbf{r}, t) = \partial_t [\nabla \times \mathbf{P}(\mathbf{r}, t)] - \nabla^2 \mathbf{M}(\mathbf{r}, t) + \nabla [\nabla \cdot \mathbf{M}(\mathbf{r}, t)]. \quad (8)$$

They form a coupled set of six nonlinear partial differential equations, which can be solved by linearization by writing

$$\mathbf{E}(\mathbf{r}, t) = \tilde{\mathbf{E}}(\mathbf{r}, t) + \mathbf{E}_{\text{ext}}(\mathbf{r}, t), \quad (9)$$

$$\mathbf{B}(\mathbf{r}, t) = \tilde{\mathbf{B}}(\mathbf{r}, t) + \mathbf{B}_{\text{ext}}(\mathbf{r}, t), \quad (10)$$

where $\mathbf{E}_{\text{ext}}, \mathbf{B}_{\text{ext}}$ are the focused external fields and $\tilde{\mathbf{E}}, \tilde{\mathbf{B}} \propto \alpha^2$ are the weak fields generated by the nonlinear interaction. The external field propagates freely in the vacuum and thus, obeys the homogeneous wave equation. It is assumed that the generated field $\tilde{\mathbf{E}}(\mathbf{r}, t)$ magnitude is much smaller than the external field, that is $|\tilde{\mathbf{E}}(\mathbf{r}, t)|, |\tilde{\mathbf{B}}(\mathbf{r}, t)| \ll |\mathbf{E}_{\text{ext}}(\mathbf{r}, t)|, |\mathbf{B}_{\text{ext}}(\mathbf{r}, t)|$. The wave equations, Eqs. (7)-(8), can then be solved using retarded potentials. The latter can be simplified furthermore within the far field approximation, assuming the distance R , where the emitted field is measured, is much larger than the interaction region L [17], that is $R \gg L$. Finally, using vector calculus identities, the solution can be simplified to [18]

$$\tilde{\mathbf{E}}_a(\mathbf{r}, t) = \frac{\omega_a^2 e^{-i\omega_a(t-R)}}{4\pi R} \int \left[-\hat{R} \times \mathbf{M}_{a,\text{ext}}(\mathbf{s}) + \mathbf{P}_{a,\text{ext}}(\mathbf{s}) - \hat{R} [\hat{R} \cdot \mathbf{P}_{a,\text{ext}}(\mathbf{s})] \right] e^{-i\omega_a \hat{R} \cdot \mathbf{s}} d^3\mathbf{s}, \quad (11)$$

$$\tilde{\mathbf{B}}_a(\mathbf{r}, t) = \frac{\omega_a^2 e^{-i\omega_a(t-R)}}{4\pi R} \int \left[\hat{R} \times \mathbf{P}_{a,\text{ext}}(\mathbf{s}) + \mathbf{M}_{a,\text{ext}}(\mathbf{s}) - \hat{R} [\hat{R} \cdot \mathbf{M}_{a,\text{ext}}(\mathbf{s})] \right] e^{-i\omega_a \hat{R} \cdot \mathbf{s}} d^3\mathbf{s}, \quad (12)$$

for photons generated at frequency ω_a . The number of photons at this frequency N_a and their spatial distribution on the surface of the detector \mathcal{S}_d can be estimated from the time-averaged Poynting vector:

$$\frac{dN_a}{d\mathcal{S}_d} = \frac{\tau}{\omega_a} |\langle \mathbf{S}_a \rangle| = \frac{\tau}{2\omega_a} \left| \text{Re} [\tilde{\mathbf{E}}_a \times \tilde{\mathbf{B}}_a^*] \right|, \quad (13)$$

where $\langle \dots \rangle$ stands for the time average and τ is the pulse duration, assuming a rectangular pulse time profile. To complete the calculation, the evaluation of $\mathbf{E}_{a,\text{ext}}$ and $\mathbf{B}_{a,\text{ext}}$ is required. Both correspond to the focused laser field close to the focal region, which is now discussed in

the context of the Stratton-Chu diffraction formulation [19, 20].

When a wave is strongly focused by a parabolic mirror, a full solution to Maxwell's equation is required [21]. For a perfectly conducting surface, the electromagnetic field generated by an opened emitting surface illuminated by an incoming laser field $\mathbf{E}_{\text{inc}}, \mathbf{B}_{\text{inc}}$ at frequency ω_a is given by the following Stratton-Chu integrals [19, 20]:

$$\begin{aligned} \mathbf{E}_{a,\text{ext}}(\mathbf{r}, t) &= \frac{1}{2\pi} \int_S \left\{ ik(\hat{\mathbf{n}} \times \mathbf{B}_{\text{inc}}) + (\hat{\mathbf{n}} \cdot \mathbf{E}_{\text{inc}}) \nabla_S \right\} G dS \\ &\quad - \frac{1}{2\pi ik} \oint_{\partial S} (\nabla_S G) [\hat{\mathbf{n}} \times (\hat{\mathbf{n}} \times \mathbf{B}_{\text{inc}})] \cdot d\boldsymbol{\ell} \quad (14) \\ \mathbf{B}_{a,\text{ext}}(\mathbf{r}, t) &= \frac{1}{2\pi} \int_S \left\{ (\hat{\mathbf{n}} \times \mathbf{B}_{\text{inc}}) \times \nabla_S G \right\} dS \\ &\quad - \frac{1}{2\pi ik} \oint_{\partial S} (\nabla_S G) (\hat{\mathbf{n}} \cdot \mathbf{E}_{\text{inc}}) \hat{\mathbf{n}} \cdot d\boldsymbol{\ell}, \quad (15) \end{aligned}$$

where S is the surface of the mirror, $\boldsymbol{\ell}$ is the tangent vector on the mirror opening ∂S , $\hat{\mathbf{n}}$ is the unit vector normal to the mirror, k is the wave vector and G is the Green's function. The parabolic shape of the mirror is accounted for in the surface integral by setting $r_S^2 = 4f(z_S + f)$ for the coordinates on the parabola (in cylindrical coordinates z and r), where f is the focal length. It is clear from Eqs. (14)-(15) that any type of incoming laser field can be used to evaluate the field at the focus, giving us the flexibility to study various field configurations. Moreover, the Stratton-Chu equations are integral solutions to Maxwell's equations and thus, should describe accurately the field of a tightly focused configuration.

The incident laser field considered here is a radially polarized Gaussian laser beam propagating in the $-\hat{z}$ direction. It is given, in the paraxial approximation, by [21]:

$$E_{\text{inc},r}(\mathbf{r}_S, t) = -E_0 \frac{2r_S}{kw_0^2} e^{-\frac{r_S^2}{w_0^2} - i\omega t - ikz_S}, \quad (16)$$

$$E_{\text{inc},z}(\mathbf{r}_S, t) = iE_0 \frac{4}{k^2 w_0^2} \left[1 - \frac{r_S^2}{w_0^2} \right] e^{-\frac{r_S^2}{w_0^2} - i\omega t - ikz_S}, \quad (17)$$

$$B_{\text{inc},\theta}(\mathbf{r}_S, t) = E_0 \frac{2r_S}{kw_0^2} e^{-\frac{r_S^2}{w_0^2} - i\omega t - ikz_S}, \quad (18)$$

where w_0 is the beam width, k is the wave number and E_0 is a normalization constant fixed from the time-average value of the Poynting vector, which is given by $E_0 = k\sqrt{\frac{2U}{\pi\tau}}$, where U is the energy per pulse. This choice of incident field is justified by the fact that radially polarized beams can be focused on a smaller region compared to linear polarization, leading to a higher field intensity close to the focal spot [22]. Presumably, this will also yield a higher number of emitted photons from mixing processes. Other polarization and field configurations will be studied in future work.

All the ingredients to compute the photon distribution have been discussed. To summarize, the first step is

the calculation of the field at the focus using Eqs. (14) and (15), for two frequencies ω_1 and ω_2 . This is performed numerically with Gauss-Legendre quadrature. In the second step, the components of \mathbf{P}_{ext} and \mathbf{M}_{ext} with frequencies $\omega_a = 2\omega_1 - \omega_2$ and $\omega_b = 2\omega_2 - \omega_1$ are extracted analytically and evaluated numerically. Finally, the generated field is computed numerically using Eqs. (11) and (12). The numerical results obtained from this procedure are now presented.

In numerical calculations, the wavelengths of the incoming laser field are set to $\lambda_1 = 820$ nm and $\lambda_2 = 780$ nm, which can be obtained from a 800 nm beam by a spectral pulse shaping technique [23]. Consequently, the radiation from mixing processes in the vacuum will be emitted at $\lambda_a \approx 864$ nm and $\lambda_b \approx 744$ nm. A broad spectrum for the incident beams, required to describe short pulses, can also be considered in principle. The effect of this will be studied in future work.

Integrated over all angles of emission, the total number of photons N is sensitive to the incident laser pulse characteristics (energy and pulse duration) as well as the parabola parameters (i.e. focusing parameters). The total number of photons N emitted at ω_a is shown in Fig. 2, as a function of the energy per pulse, for different focal lengths. Clearly, for smaller focal lengths, the number of photons can be enhanced by many orders of magnitude due to the larger focused field. This is similar to the results found in [15]. The scaling of N with the pulse energy (U) shown in figure 2 can be obtained analytically from the scaling of the field and the expressions for the emitted radiation: the number of photons scales like $N \propto U^3/\tau^2$, which explains the rapid rise of the photon production rate with the energy per pulse.

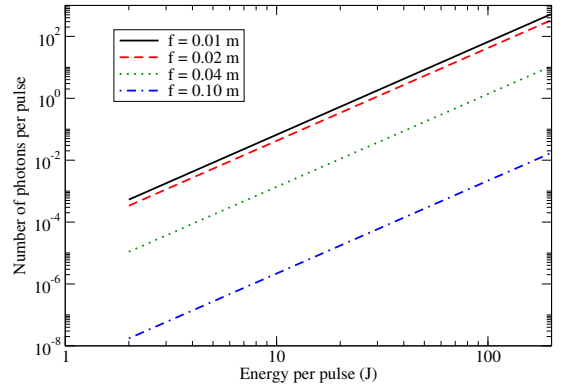


FIG. 2: Total number of photons emitted at $\omega_a = 2\omega_1 - \omega_2$, as a function of the energy per pulse for focal length $f = 0.01, 0.02, 0.04$ and 0.10 m. The size of the parabola aperture is $r_{\text{max}} = 0.08$ m. Incident pulse: $\lambda_1 = 820$ nm and $\lambda_2 = 780$ nm with a Gaussian profile $w_0 = 0.03$ m and pulse duration $\tau = 30$ fs.

In the following numerical calculations, we consider a 1 PW laser, which is now available [2], with a pulse length

of $\tau = 30$ fs and an energy per pulse of $U = 30$ J. The total number of photons emitted at ω_a as a function of focal length (f) and aperture size (r_{\max}) is shown in Fig. 3. This result demonstrates that the number of photons emitted saturates at a certain value of r_{\max} where the non-reflected tail of the Gaussian beam is negligible. More interesting however is the non-linear increase of the number of emitted photons as the focal length is decreased or as the aperture size is increased: this effect is caused by the higher field strength attained as f becomes smaller and r_{\max} becomes larger. This can be used to enhance the signal from wave mixing in vacuum.

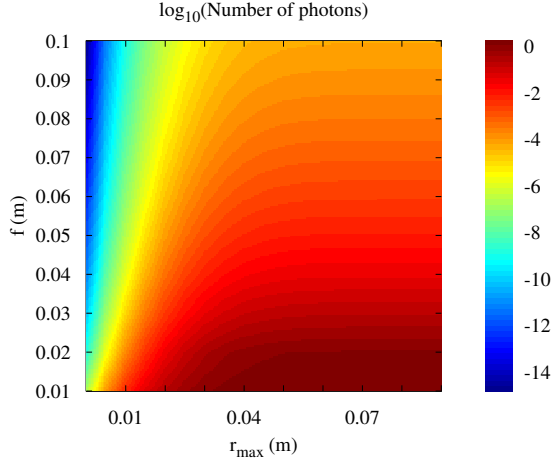


FIG. 3: Total number of photons emitted at $\omega_a = 2\omega_1 - \omega_2$, as a function of the focal length f and the parabola aperture r_{\max} . Incident pulse: $\lambda_1 = 820$ nm and $\lambda_2 = 780$ nm with a Gaussian profile $\omega_0 = 0.03$ m, pulse duration $\tau = 30$ fs and energy $U = 30$ J.

In Fig. 4, the photon distribution as a function the angle θ from the optical axis of the parabola (the z -axis) is presented with some optimized parameters. In both mixing cases ($\lambda_{a,b}$), most of the photons are emitted in the range $[40^\circ, 90^\circ]$. This should guide future experiments for optimizing the detection system.

The numerical results generally show that in a certain parameter range, when the energy per pulse is large, the focal length is small and when the aperture size is large, a detectable number of photons can be emitted by vacuum mixing processes. For instance, it is claimed that the planned Appolon high-intensity infrastructure should deliver $\tau \sim 15$ fs pulses at 10 PW, for an energy per pulse of 150 J [24]. Using a beam width of $w_0 = 0.2$ m, $f = 0.02$ m and $r_{\max} = 0.15$ m, it would be possible to produce $N \approx 6.5$ photons per shot in our tightly focused geometry.

The main advantage of this geometry however pertains to the alignment and synchronization of the beams: in most scenarios (see [5, 13] for instance), one considers the crossing of many laser beams. It is a very challenging technical task to align and synchronize many highly fo-

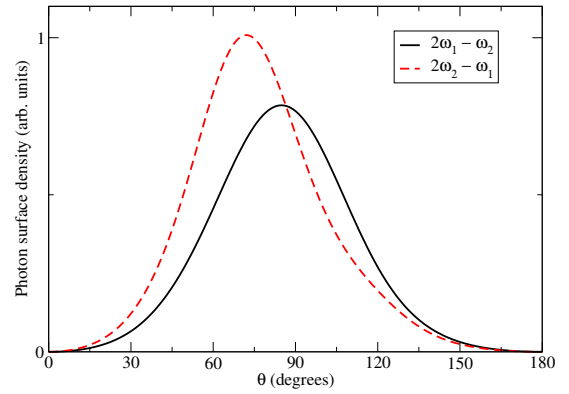


FIG. 4: Photon density as a function of the angle of emission θ with respect to the optical axis of the parabolic mirror of aperture $r_{\max} = 0.08$ m and focal length $f = 0.02$ m. Incident pulse: $\lambda_1 = 820$ nm and $\lambda_2 = 780$ nm with a Gaussian profile $\omega_0 = 0.03$ m, pulse duration $\tau = 30$ fs and energy $U = 30$ J.

cused counter-propagating short pulse laser beams while preserving a high intensity at the interaction region. This is because in order to obtain the intensity required to observe wave mixing in vacuum with lasers of 1 - 10 PW, the laser has to be focused on a very small focal spot, the size of a wavelength ($\lambda_{\text{focal spot}} \sim \lambda$). The technique presented in this letter circumvents these complications because a single incident beam can be used. Then, the mixing occurs at the focus between its different frequency components and this process can be optimized by using a spectral pulse shaping technique [23]. A more detailed analysis of this geometry, including the effect of short pulse spectra, will be presented in future work.

The authors would like to thank Drs. S. Fourmaux, K. Otani, S. Payeur and Prof. J.-C. Kieffer for many valuable discussions on this subject.

* francois.fillion@emt.inrs.ca

† catherine.lefebvre@emt.inrs.ca

‡ steve.maclean@emt.inrs.ca

- [1] G. A. Mourou, T. Tajima, and S. V. Bulanov, Rev. Mod. Phys. **78**, 309 (2006).
- [2] A. Di Piazza, C. Müller, K. Z. Hatsagortsyan, and C. H. Keitel, Rev. Mod. Phys. **84**, 1177 (2012).
- [3] G. V. Dunne, From fields to strings: Circumnavigating theoretical physics **1**, 445 (2005).
- [4] N. Rozanov and D. Book, Zh. Eksp. Teor. Fiz **103**, 1996 (1993).
- [5] F. Moulin and D. Bernard, Optics Communications **164**, 137 (1999).
- [6] D. Bernard, F. Moulin, F. Amiranoff, A. Braun, J. Chambaret, G. Darpentigny, G. Grillon, S. Ranc, and F. Perone, The European Physical Journal D - Atomic, Molecular, Optical and Plasma Physics **10**, 141 (2000).

- [7] E. Iacopini and E. Zavattini, *Physics Letters B* **85**, 151 (1979).
- [8] W. Dittrich and H. Gies, in *Frontier Tests of QED and Physics of the Vacuum*, edited by E. Zavattini, D. Bakalov, and C. Rizzo (1998) p. 29, hep-ph/9806417.
- [9] T. Heinzl, B. Liesfeld, K.-U. Amthor, H. Schwöerer, R. Sauerbrey, and A. Wipf, *Optics Communications* **267**, 318 (2006).
- [10] R. Battesti and C. Rizzo, *Reports on Progress in Physics* **76**, 016401 (2013).
- [11] Y. J. Ding and A. E. Kaplan, *Phys. Rev. Lett.* **63**, 2725 (1989).
- [12] S. Payeur, S. Fourmaux, B. E. Schmidt, J. P. MacLean, C. Tchervenkov, F. L  gar  , M. Pich  , and J. C. Kieffer, *Applied Physics Letters* **101**, 041105 (2012).
- [13] E. Lundstr  m, G. Brodin, J. Lundin, M. Marklund, R. Bingham, J. Collier, J. T. Mendon  a, and P. Norreys, *Phys. Rev. Lett.* **96**, 083602 (2006).
- [14] B. King and C. H. Keitel, *New Journal of Physics* **14**, 103002 (2012).
- [15] Y. Monden and R. Kodama, *Phys. Rev. Lett.* **107**, 073602 (2011).
- [16] Z. Bialynicka-Birula and I. Bialynicki-Birula, *Phys. Rev. D* **2**, 2341 (1970).
- [17] For a tightly focused laser field, this is a few wavelengths $L \sim \lambda$.
- [18] B. King, A. Di Piazza, and C. H. Keitel, *Phys. Rev. A* **82**, 032114 (2010).
- [19] J. A. Stratton and L. J. Chu, *Phys. Rev.* **56**, 99 (1939).
- [20] P. Varga and P. T  r  k, *J. Opt. Soc. Am. A* **17**, 2081 (2000).
- [21] Y. I. Salamin, *New Journal of Physics* **8**, 133 (2006).
- [22] R. Dorn, S. Quabis, and G. Leuchs, *Phys. Rev. Lett.* **91**, 233901 (2003).
- [23] P. Lassonde, F. Th  berge, S. Payeur, M. Ch  teauneuf, J. Dubois, and J.-C. Kieffer, *Opt. Express* **19**, 14093 (2011).
- [24] G. Ch  riaux, F. Giambruno, A. Fr  neaux, F. Leconte, L. P. Ramirez, P. Georges, F. Druon, D. N. Papadopoulos, A. Pellegrina, C. Le Blanc, I. Doyen, L. Legat, J. M. Boudenne, G. Mennerat, P. Audebert, G. Mourou, F. Mathieu, and J. P. Chambaret, *AIP Conference Proceedings* **1462** (2012).